Site trimer percolation on square lattices

W. Lebrecht, E. E. Vogel,* and J. F. Valdés
Departamento de Ciencias Físicas, Universidad de La Frontera, Casilla 54-D, Temuco, Chile

A. J. Ramirez-Pastor, P. M. Centres, M. I. González, and F. D. Nieto
Departamento de Física, Instituto de Física Aplicada, Universidad Nacional de San Luis-CONICET, Ejército de los Andes 950, D5700HHW, San Luis, Argentina

(Received 29 April 2015; revised manuscript received 19 June 2015; published 23 July 2015)

Percolation of site trimers (k-mers with $k = 3$) is investigated in a detailed way making use of an analytical model based on renormalization techniques in this problem. Results are compared to those obtained here by means of extensive computer simulations. Five different deposition possibilities for site trimers are included according to shape and orientation of the depositing objects. Analytical results for the percolation threshold p_c are all close to 0.55, while numerical results show a slight dispersion around this value. A comparison with p_c values previously reported for monomers and dimers establishes the tendency of p_c to decrease as k increases. Critical exponent ν was also obtained both by analytical and numerical methods. Results for the latter give values very close to the expected value 4/3 showing that this percolation case corresponds to the universality class of random percolation.

DOI: 10.1103/PhysRevE.92.012129 PACS number(s): 64.60.ah, 64.60.De, 68.35.Rh, 05.10.Ln

I. INTRODUCTION

Percolation is a very active field of research and applied to a diversity of phenomena in physics as, for example, metal-insulator phase transitions, fluid flow in random media, sol-gel transitions, and failures in complex networks [1,2]. Percolation models have also been used to understand many chemical, biological, and social phenomena [2–4].

Models to attempt to explain the percolation properties of different two-dinensional (2D) systems can allow different features as can be seen from the following examples. The percolation properties of cars parking in a marked parking lot can be tackled as monomeric percolation on a lattice: a single object is deposited on a geometrically determined position. If the parking lot has just one level we must add another condition to this kind of percolation: nonoverlapping. If the cars now park anywhere in the parking lot (no geometrical marks) no lattice needs to be considered. On the other hand, if we consider painting with a spray device we do not only want percolation but we need full coverage of randomly deposited overlapping objects.

In the present paper we consider trimers (polymers or k-mers with $k = 3$ in a more general conception) where three objects are simultaneously deposited onto a surface. An example is provided by triatomic molecules which tend to self-organize to minimize energy which leads to a long-range ordering in many cases: this means the presence of a lattice. Even when only short-range ordering is possible an approximate lattice is always present.

All of the previous introduction is to say that in the present work we consider the deposition of trimers whose equilibrium positions are at least approximately described by a square lattice. Such trimer could be any object occupying a slot that can be considered as formed by three pieces. Just as a way of thinking we can mention the analog to triatomic molecules which can be formed by atoms along a straight line (like CO_2, for instance) or in an angular way (like H_2O, for instance). This is an approximate model and some allowance has to be made to consider cases of different interatomic distances or angles not exactly at 90° as in the square lattice. This is the case of the water molecule whose angle is about 105°, which is halfway between a square lattice and a triangular lattice. Actually, the water molecule has been considered as occupying sites in a triangular lattice with an angle of 120° [5]. Actually a better realization for a 90° angle is given by H_2S and H_2Se whose angles are about 92° and 91°, respectively. The case of nonoverlapping trimers in the form of triangles (and hexagons) deposited randomly over a 2D surface [6] bears something in common with these examples, but this is only with respect to the number of elements defining the geometrical object. However, the shape of the objects and the approach used in the present are different.

Percolation theory was derived for periodic lattices of sites (bonds) which are occupied with probability p or empty (nonoccupied) with probability $(1 - p)$ [1,7]. In the thermodynamic limit p coincides with the coverage of the lattice or fraction of occupied sites (bonds). Nearest-neighboring occupied sites (bonds) form structures called clusters. Quantities relevant to percolation will depend on the concentration of elements and geometry of the lattice. When the concentration is low, sites are either isolated or in small clusters of adjacent elements. As p increases, the average size of the clusters increases monotonically. The probability that a cluster percolates connecting one extreme of the lattice to the opposite extreme increases monotonically with p. For finite-size lattices there is a probability for percolation as a function of p. This function tends to a step function in the thermodynamic limit; the critical concentration p_c at which the step occurs is known as the percolation threshold p_c. The percolation transition is a second-order phase transition and can be characterized by well-defined critical exponents.

More general percolation problems can be formulated by including deposition of elements occupying more than one

*To whom all correspondence should be addressed.

site (bond) [8–12]. In Refs. [8,9], the percolation behavior for particles that occupy several k contiguous lattice sites (k-mers) with a length in the interval $k = 1, \ldots, 15$ has been numerically studied. The authors found that, for straight and tortuous k-mers deposited on 2D square lattices, the percolation threshold exhibits an exponentially decreasing behavior as a function of the k-mer size. Actually, the results reported below confirm this tendency for all possible trimers. This feature was also observed for straight k-mers on 3D cubic lattices [10]. A nonmonotonic size dependence was observed for the percolation threshold of large straight k-mers on 2D square lattices, which decreases for small particles sizes, goes through a minimum at $k \approx 13$–16, and finally increases for larger segments [11,12]. In all the studied cases, the problem was shown to belong to the random percolation universality class.

In most of the cases mentioned above [8–11], the objects are deposited randomly and irreversibly. This filling process, known as random sequential adsorption model, leads to intermediate states characterized by an isotropic distribution of the directions of the deposited objects. The effect of anisotropy (or k-mer alignment) on percolation has been recently investigated for the case of dimers [13] and straight rigid k-mers on square lattices [12,14,15]. The studies in Refs. [12–15] represent an important step in the understanding of the percolating properties of anisotropic conductors. From the experimental point of view, it is important to consider the contribution of the aspect ratio of the k-mers to the electrical conductivity of anisotropic composites made of small conducting rods on an insulating matrix; such a role has been emphasized by various authors [16–19].

Despite of the number of contributions to the multisite percolation problem, there are many aspects which still need to be explored. In fact, most of the studies have been based on computer simulations and the obtained results have not been corroborated yet by analytical methods. In recent works from our group [20,21], bond and site dimer percolation have been studied by using analytical approximations based on exacts results for small cells that can be extrapolated to larger sizes. In this context, the main objective of the present work is to extend such results to larger objects like the trimers considered here. The study is a natural continuation of our previous work [20,21] and focuses on the percolation properties of site trimers with *all possible*shapes and orientations. The study of trimer phases is not only of analytical interest, but also of considerable practical importance in surface physics [5,6,22–24].

The paper is organized as follows. In Sec. II, the basic definitions are given along with the general basis of the computer simulations. Results are presented in Sec. III. Finally, the conclusions are drawn in Sec. IV.

II. MODEL

A. Trimer deposition

We assume a trimer formed by three bound objects which can be along a straight line or at an angle. For simplicity, we assume equal distances between objects and angles of 180° (linear trimers) or 90° (angular trimers). Deposition is irreversible, nonoverlapping, and always assumed parallel to the deposition surface (substrate). Trimers are illustrated in Fig. 1 as formed by three equal disks bound by short black bars. The substrate can be represented by a square lattice with a lattice constant equal to the distance between neighboring objects in the trimer. Then several possible deposition possibilities can be studied as follows.

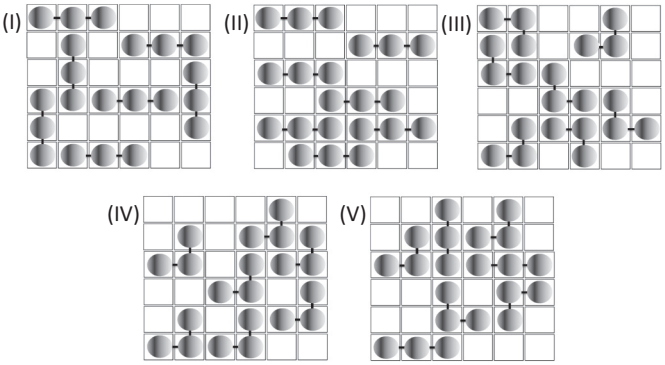

FIG. 1. Five possible ways for trimer deposition on a square lattice. (I) Straight: a lineal trimer can match the lattice constant both horizontally and vertically. (II) Nematic: an oriented lineal trimer can have directional depositions only, horizontal in the present case. (III) Angular: angular trimers can deposit in any of the four equivalent possibilities. (IV) Arrow: oriented angular trimers can deposit in only one of the four possibilities. (V) Tortuous: combination of (I) and (III) under equal probability of deposition for each of the six possibilities. In all the illustrated cases a percolating occupancy is shown.

(i) Case I: Straight. Linear trimers can be deposited either in the left-right direction (horizontal) or up-down direction (vertical); this is illustrated in Fig. 1(I).

(ii) Case II: Nematic. A polarization is imposed in such way that just one direction is allowed for linear trimers; horizontal is the case illustrated in Fig. 1(II).

(iii) Case III: Angular. 90° trimers are deposited in any of the four possible orientations as illustrated in Fig. 1(III).

(iv) Case IV: Arrow. A polarization is imposed so only one of the previous four possibilities prevails as illustrated in Fig. 1(IV). In a sense this is also a nematic case since it favors a particular direction.

(v) Case V: Tortuous. The six deposition possibilities comprised upon combining cases I and III are considered; this is shown in Fig. 1(V). Cases II and IV could be achieved by means of chemical transport, applied electric fields, or applied magnetic fields, depending on the nature of the trimers. In the cases I, III, and V the deposition scans all possible orientations without biasing any one in particular.

B. Renormalization cell

We assume that the deposition takes place on a small lattice of dimensions L_x and L_y along the horizontal and vertical directions, respectively. The unit of measure is the distance between two nearest neighbors on the lattice. Thus this finite lattice or cell has $M = L_x \times L_y$ individual sites, where we can define $L = L_x = L_y$ for symmetric cells and $L = (L_x + L_y)/2$ for nonsymmetric cells. Each trimer occupies simultaneously three sites according to its shape

and orientation. Once deposited the trimer remains "frozen" on the substrate without dissociations or migrations. For a deposition of ℓ trimers the *coverage*is $p = 3\ell/M$. For any given p different combinations of the 3ℓ trimers are possible each one of which will be called a *configuration.*For any polymer (k-mer) we can think of successive depositions in a progressive way going over different coverage values, namely, $p = 0,3/M,\ldots,3\ell/M$. This is valid for any of the five depositions, considering cells of different M values. Just one percolating configuration for each case is shown in Fig. 1, but the reader can realize that by means of variations in the depositions of the trimers other configurations can be reached for the same p value, some of which may not lead to percolation.

From what is known of percolation theory the probability of percolation increases with coverage p. One of the main goals of the present work is to obtain *all* the configurations for a given p, for each deposition case. From there, we can analytically get the percolation probabilities for several M sizes. Then by means of scaling methods upon progressive L values we will estimate the percolation threshold for each deposition case in the thermodynamic limit. This progressive analysis also allows one to get an approximation to the critical exponents is a way similar to what was done in the case of site dimer percolation [20]; we will concentrate here on the exponent ν.

For each cell a protocol is defined to cover exhaustively for possible depositions going from one trimer ($\ell = 1$) to the maximum possible number of trimers for each deposition case. We illustrate in Fig. 2 the six possible initial configurations corresponding to the tortuous case (V in the enumeration above). This is a nested protocol where we first vary the pivot site position (i,j), being j the column index which corresponds to the inner nest; for each of such positions these six possible trimer shapes $K = 1$ through 6 are successively tried as presented in Fig. 2 for $\ell = 1$, at the initial position (1,1). The numbering given to these shapes is arbitrary and it does not matter since all six shapes have exactly the same probability (1/6) in the exhaustive enumeration. If at any instant the trimer corresponding to a given shape lays outside

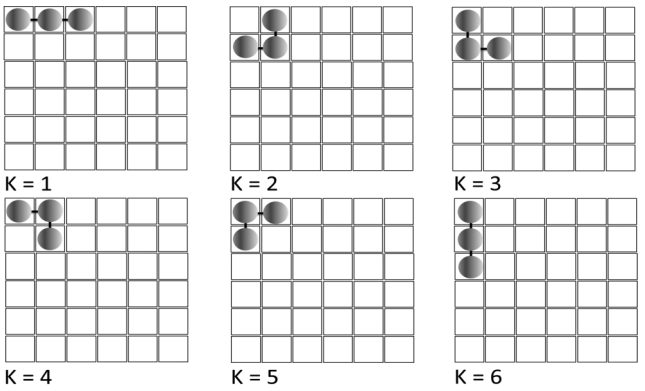

FIG. 2. Six possible depositions of trimers associated to case V for a cell $M = 36$ at the initial deposition site (1,1) ($i = 1$, $j = 1$). Each of these figures illustrates the first deposition of each one of these shapes; then the deposition site (i,j) sweeps the entire cell looking for allowed depositions.

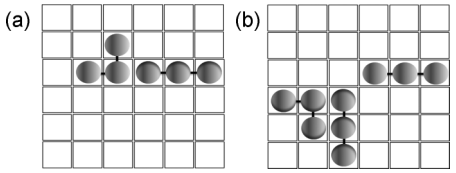

FIG. 3. (a) Deposition of two trimers for $\ell = 2$, $K1 = 2$, (2,2), and $K2 = 1$, (3,4) on a square lattice of size $M = 36$. This deposition is followed by $(i2, j2)$ going over (3,5) and (3,6) which are forbidden; it continues to (4,1), (4,2), etc. (b) Deposition of three trimers, namely $\ell = 3$ for $K1 = 1$ (3,4), $K2 = 4$ (4,1), and $K3 = 6$ (4,3). Again here the inner nest is run until the last possible deposition position before moving the previous deposition.

the cell, such configuration is discarded going onto the next possible one. In this way we find all the $F_{\ell,K}$ configurations corresponding to $\ell = 1$, namely $F_{1,1} = 24$, $F_{1,2} = 25$, $F_{1,3} = 25$, $F_{1,4} = 25$, $F_{1,5} = 25$, and $F_{1,6} = 24$. This makes a total of 148 configurations for one trimer deposition in the tortuous case, all of them nonpercolating.

The next step is to consider $\ell = 2$, two trimers, which requires two equally likely independent shapes $K1$ and $K2$, at two different deposition sites $(i1, j1)$ and $(i2, j2)$, where $(i1, j1)$ run from (1,1) to (6,6), while $(i2, j2)$ runs from the values of previous indices to (6,6). This is illustrated in Fig. 3(a) for $\ell = 2$, $K1 = 2$, (2,2), and $K2 = 1$, (3,4). If at any instant the trimer corresponding to a given shape lays outside the cell or over any already occupied position, such configuration is discarded and the most inner index is increased. The configurations in terms of $F_{2,K1}$ are now $F_{2,1} = 1289$, $F_{2,2} = 1379$, $F_{2,3} = 1414$, $F_{2,4} = 1477$, $F_{2,5} = 1497$, and $F_{2,6} = 1620$. This makes a total of 8676 configurations for the deposition of two trimers in the tortuous case, with only six of them percolating.

Then we move onto three trimers deposition, namely $\ell = 3$ as illustrated in Fig. 3(b) for $K1 = 1$ (3,4), $K2 = 4$ (4,1), and $K3 = 6$ (4,3). The counting now yields $F_{3,1} = 41905$, $F_{3,2} = 39846$, $F_{3,3} = 41572$, $F_{3,4} = 45006$, $F_{3,5} = 46094$, and $F_{3,6} = 47693$. The total number of configurations for $\ell = 3$ is 262116, from which 3812 percolate in the tortuous case.

This process can be continued until $\ell = 6$ for the tortuous case. Similar procedure was applied separately to all the other deposition cases.

Consider any of the six shapes $K = 1$ through 6 which requires the simultaneous occupancy of three connected sites. In Fig. 4 we illustrate it by means of shape $K = 1$ but the same argument applies for the other five shapes in Fig. 2. We consider the four possibilities: (a) the three sites available for trimer occupancy; (b) two sites available and one site forbidden (occupied or out of bounds marked with an X in Fig. 4) with degeneracy 3; one site available and two sites forbidden with degeneracy 3; (d) the three sites forbidden. Just one of these configurations will lead to the simultaneous occupancy of the three sites, with a weight $t = p^3$ for coverage p. The other seven possibilities will imply that this shape cannot be accommodated in the slot under consideration, so the weight for nontrimer deposition is given by $3p^2(1-p) + 3p(1-p)^2 + (1-p)^3 = 1 - p^3 = 1 - t$.

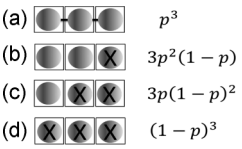

FIG. 4. Probabilities of occupancy for the first shape in Fig. 2, namely three adjacent horizontal sites: (a) each one of the three sites is available at an occupancy p each; (b) two sites are available and one site forbidden (marked with an X), with degeneracy 3; (c) one site is available and two sites are forbidden, with degeneracy 3; (d) the three sites are forbidden.

For any large enough value of p there are configurations that percolate among the total number of possible configurations for any k-mer deposition. The ratio between these two quantities represents the percolation probability which is a function of p tending to a step function at a critical value p_c in the thermodynamic limit.

One of the main goals of the present work is to obtain *all* the configurations for a given p, for each deposition case. From there, we can analytically get the point of the curve behaving like the percolation threshold for several M sizes. Then by means of scaling methods upon progressive L values we will estimate the percolation threshold in the thermodynamic limit for each deposition case. This progressive analysis also allows to get an approximation to the critical exponents is a way similar to what was done in the case of site dimer percolation [20]; we will concentrate here on the exponent ν.

A percolation cluster is formed by all the sites that connect the cell from one extreme to the opposite one (from left to right when using the cell method below). Such cluster (also known as percolation trajectory) is formed by ℓ trimers satisfying a necessary condition for percolation: $\ell \geqslant \ell_{\min}$. For smaller values of ℓ, percolation is not possible. At the precise value $\ell = \ell_{\min}$ at least one configuration leads to percolation. The number of percolating trajectories for any given ℓ will render the weight of such concentration of trimers as it will be calculated and tabulated below. This process goes over until saturation, which is reached for $\ell = \ell_{\max}$. It can be noticed that each size L has a well defined pair of values for $\ell_{\min}$ and $\ell_{\max}$.

As discussed above $t = p^3$ represents the occupancy probability for a trimer and $1-t$ is the probability that such slot cannot be occupied by a trimer. Generalizing the example studied above for the tortuous case we can say that the total number of configurations for ℓ trimers in the X case ($X = I, II, III, IV, V$) of deposition in a lattice of size M is $H^X_{\ell,M}$. From these configurations, $G^X_{\ell,M}$ percolate. For simplicity we will drop the index M.

The analytical percolation probability for any given t (or p) and L is the ratio between the number of percolating configurations G^X_ℓ to the total number of configurations H^X_ℓ for each cell, and for each deposition case:

$$g^X_L(t) = \frac{\sum_{\ell=\ell_{\min}}^{\ell=\ell_{\max}} G^X_\ell t^\ell (1-t)^{\ell_{\max}-\ell}}{\sum_{\ell=0}^{\ell=\ell_{\max}} H^X_\ell t^\ell (1-t)^{\ell_{\max}-\ell}} = f^X_L(p), \qquad (1)$$

where $\ell_{\min} = [L_x/3]$, $\ell_{\max} = [M/3]$; the bracketed ratio $[P/Q]$ represents the approximation to the upper integer whenever the ratio P/Q is not an exact integer.

The task is now to evaluate the coefficients H^X_ℓ and G^X_ℓ in an exact way for each cell size and deposition case. This is accounted for by a computer program which goes over *all* possible deposition possibilities, detecting percolation. In this way all configurations for any given ℓ are counted and all percolating configurations are separately counted in order to get the G^X_ℓ coefficients. This process is extremely time consuming as cell sizes grow which imposes a practical limit for the maximum M value to be considered.

At this point we illustrate the results of this process for $M = 36$ ($L = 6$). Here $\ell_{\min} = 2$ for cases I, II, and V, while $\ell_{\min} = 3$ for cases III and IV. On the other hand, $\ell_{\max} = 12$ for all cases except IV where $\ell_{\max} = 9$. This last exception is topological and unique for this case, where a full coverage is impossible. Table I(a) lists coefficients H^X_ℓ and G^X_ℓ for deposition cases I, II, III, and V defined above. Table I(b) completes the series for $M = 36$ with case IV. Tables for other sizes M were constructed along this same procedure.

C. Numerical calculations

In the case of present numerical simulations the depositions of the trimers follow the same five possibilities already described above. The main difference with respect to the renormalization cell is that the lattice sizes considered here are much larger making exact enumeration nearly impossible. However, if a large enough number of random configurations is visited for each p value then the ratio defined by Eq. (1) can be obtained in an approximate way. The larger the set of random configurations used to numerically calculate the percolation function the better the approximation is.

Each simulation run consists of the following two steps: (a) the construction of the lattice for the desired fraction p of occupied sites, and (b) the cluster analysis using the Hoshen and Kopelman algorithm [25]. In the last step, the existence of a percolating island is determined. For this purpose, the probability $R^X_{L,Y}(p)$ that a lattice composed of $L \times L$ sites percolates at concentration p can be defined [1]. Here, the following definitions can be given according to the meaning of Y [26].

$R^X_{L,R(D)}(p)$: the numerical probability of finding a rightward (downward) percolating cluster of type X trimers ($X = I, II, III, IV, V$).

$R^X_{L,I}(p)$: the numerical probability of finding a cluster of type X trimers which percolates both in a rightward and in a downward direction.

$R^X_{L,U}(p)$: the numerical probability of finding either a rightward or a downward percolating cluster of type X trimers.

$R^X_{L,A}(p) = \frac{1}{2}[R^X_{L,U}(p) + R^X_{L,I}(p)]$.

A total of m^X_L independent runs of such two steps procedure were carried out for each X case and each lattice size L. From these runs a number $m^X_{L,Y}$ of them present a percolating cluster. This is done for the desired criterion among $Y = \{R, D, I, U, A\}$. Then, $R^X_{L,Y}(p) = m^X_{L,Y}/m^X_L$ is defined and the procedure is repeated for different values of L, p, and trimer deposition (cases I–V). A set of $m^X_L = 10^5$ independent random samples is numerically prepared for several values of the system size ($L = 384, 768, 1152, 1536, 1920$). As it can be appreciated this represents extensive calculations to cope with the trimer percolation problem from the numeric point of

TABLE I. (a) Coefficients H_ℓ^X and G_ℓ^X where X is associated to trimers of the cases I, II, III, and V on a square cell of size $M = 36$. (b) Coefficients H_ℓ^{IV} and G_ℓ^{IV} associated to arrow trimers on a square cell of size $M = 36$.

ℓ	*Polynomial*	H_ℓ^I	G_ℓ^I	H_ℓ^{II}	G_ℓ^{II}	H_ℓ^{III}	G_ℓ^{III}	H_ℓ^V	G_ℓ^V
					(a)				
0	$(1-t)^{12}$	1	0	1	0	1	0	1	0
1	$t(1-t)^{11}$	48	0	24	0	100	0	148	0
2	$t^2(1-t)^{10}$	924	6	246	6	3952	0	8676	6
3	$t^3(1-t)^9$	9376	288	1400	136	80068	972	262116	3812
4	$t^4(1-t)^8$	55378	5367	4815	1191	903814	61172	4454292	319089
5	$t^5(1-t)^7$	198112	46080	10224	5056	5809648	1230872	43732304	9316072
6	$t^6(1-t)^6$	432408	191908	13236	10596	21017436	9684026	246232904	111171662
7	$t^7(1-t)^5$	565504	388924	10224	10224	41094868	30345152	767045820	552117100
8	$t^8(1-t)^4$	424270	371787	4815	4815	40254432	37084564	1234332462	1122288219
9	$t^9(1-t)^3$	169744	164104	1400	1400	17240936	17026500	911325936	898421292
10	$t^{10}(1-t)^2$	31509	31311	246	246	2462672	2461728	249479639	249386239
11	$t^{11}(1-t)$	1317	1317	24	24	70208	70208	16453726	16453726
12	t^{12}	64	64	1	1	162	162	80092	80092

(b)

ℓ	*Polynomial*	H_ℓ^{IV}	G_ℓ^{IV}
0	$(1-t)^9$	1	0
1	$t(1-t)^8$	25	0
2	$t^2(1-t)^7$	244	0
3	$t^3(1-t)^6$	1195	16
4	$t^4(1-t)^5$	3145	246
5	$t^5(1-t)^4$	4431	1149
6	$t^6(1-t)^3$	3161	1868
7	$t^7(1-t)^2$	1007	935
8	$t^8(1-t)$	111	111
9	t^9	2	2

view. From there on, the finite-scaling theory can be invoked to determine the percolation threshold and the critical exponent ν with a reasonable accuracy [1,26,27].

The deposition in the numeric case is done as it follows, where we consider the tortuous case as an example. A site (i, j) is randomly chosen. Then we randomly select any of the four equivalent neighboring positions (factor 1/4). At this point the analysis forks in two equivalent possibilities: horizontal or vertical occupancy (multiplicity 2). Let us pick the former one. Then any of these two occupied sites has three equivalent sites to be selected to complete the trimer giving a total of six equivalent possibilities (factor 1/6). From them, two lead to an horizontal trimer equivalent to $K = 1$ in Fig. 2 (degeneracy 2), while each of the other four trimers lead to each of the angular trimers, $K = 1$ through 5 (degeneracy 1). When we go back to the fork point above we can do exactly the same analysis for the vertical occupancy, getting now two possibilities for the vertical trimer $K = 6$ and one additional possibility for each of the angular trimers, thus completing a degeneracy 2 for any of the shapes in Fig. 2. If we now combine the probabilities for any of the depositions they yield $(1/4) \times 2 \times (1/6) \times 2 = 1/6$, exactly as assumed in the renormalization cell method above. This makes the two methods equivalent which allows one to compare their results towards the thermodynamic method.

In the case of renormalization deposition the exhaustive enumeration of configurations allows one to assign a weight to each one corresponding to its share of the total universe of possible configurations. In the case of numerical calculations a large number of random depositions will assign the weight to each configuration. Our hypothesis is that these two approaches should converge towards the thermodynamic limit and the results presented next seem to prove it.

III. RESULTS

We will present below results for percolation thresholds and critical exponents ν for all deposition cases choosing I and III as examples to give the details of the procedures. We will also report the universality class of this kind of percolation. The presentation is arranged so the results obtained by the renormalization cell (analytical techniques) go first and they are immediately followed by the results of the numerical calculations.

A. Percolation threshold

Analytical. Let us go back to the analytical approach based on renormalization cells of increasing sizes. Following Eq. (1) it is possible to obtain the percolation function for any deposition case and size M. The coefficients for the deposition cases I and III and $M = 36$ are given in Table I(a). The corresponding curves as functions of p are given in Fig. 5.

Once the percolation function is obtained we can use two different methods to obtain the corresponding percolation threshold for each case and size [20]: (A) inflection point of the

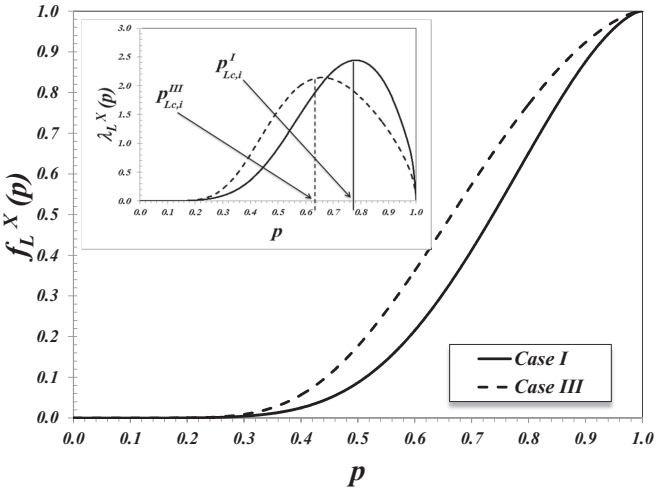

FIG. 5. Percolation functions for cell of size $M = 36$ and deposition cases $X = I$ and $X = III$. The inset shows the first derivatives of the corresponding percolating functions maximizing at the critical concentration $p_{Lc,i}^X$, where the subindex i refers to the inflection method discussed in the text as method A.

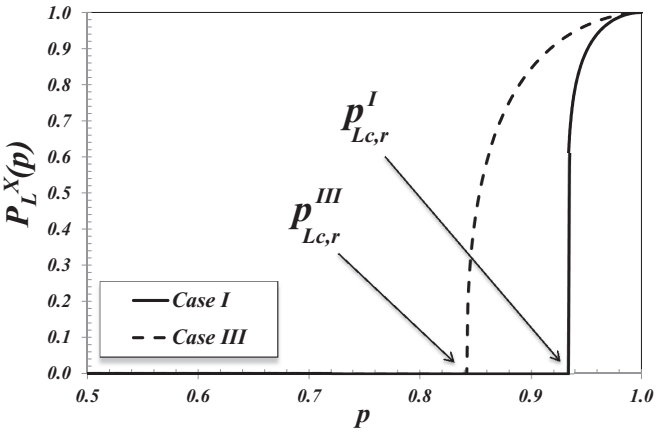

FIG. 6. Accumulated function constructed after 50 iterations in the way described by Eq. (3) in the text. Values for which this function vanishes yield the corresponding percolation thresholds for depositions I and III.

percolation function $p_{Lc,i}^X$ and (B) renormalization techniques $p_{Lc,r}^X$.

Method A is based on the idea that the percolation function tends to a step function in the thermodynamic limit; hence its first derivative should tend to diverge there. This is represented in the inset of Fig. 5 for cell of size $M = 36$.

Method B is based on the assumption that at the critical concentration the function is equal to the probability of occupancy of a single object (renormalization techniques). Then,

$$f_L^X\left(p_{Lc,r}^X\right) = p_{Lc,r}^X. \tag{2}$$

Alternatively, $p_{Lc,r}^X$ can be determined upon constructing a composed function which is called $P_L^X(p)$ by means of successive approximations based on the functions $f_L^X(p)$ [28,29]:

$$P_L^X(p) = \prod_{k=1}^{k=n} f_{k,L}^X(p) \quad (n \to \infty), \tag{3}$$

with

$$f_{k,L}^X(p) = f_L^X\left(f_L^X\left(f_L^X(p)\ldots\right)\right) \quad (k \text{ times}), \tag{4}$$

where the index k means the number of iterations for the function $f_L^X(p)$. In this way, $P_L^X(p)$ is a function that goes to zero for values of p below the percolation threshold and tends to unity over the percolation threshold.

The rationale here is simple: powers of numbers less than one tend to zero as the power increases, so $P_L^X(p)$ should go to zero for p values less than a fixed point p_f. But, this point happens precisely at the step function for percolation in the thermodynamic limit; then $p_{c,r}^X = p_f$. This approach is based in well-known renormalization techniques [30,31] adapted to the present case in a way analogous to the treatment presented in Fig. 11 of Ref. [1]. Such composed function was obtained numerically for size $M = 36$ as presented in Fig. 6 after 50 iterations, for cases I and III. The points at which these functions vanish correspond to the percolation thresholds: $p_{6c,r}^I = 0.842$ and $p_{6c,r}^{III} = 0.933$.

The same procedure employed in Figs. 5 and 6 can now be applied to the other three deposition cases. This was done for $M = 30$, 36, 42, and 49 for all five deposition cases and their results will be discussed below.

With the values of the percolation thresholds for different L values we attempt a scaling approach valid for small cells by means of [20,32]:

$$p_{Lc,r(i)}^X = p_{\infty c,r(i)}^X + L^{-1/\nu}\left(a_{r(i)}^X + b_{r(i)}^X L^{-1} + c_{r(i)}^X L^{-2} + d_{r(i)}^X L^{-3} + \cdots\right), \tag{5}$$

where $a_{r(i)}^X$, $b_{r(i)}^X$, $c_{r(i)}^X$, $d_{r(i)}^X$, ... are adjustable parameters.

If we define

$$\chi_{Lc,r(i)}^X = L^{-1/\nu}\left(a_{r(i)}^X + b_{r(i)}^X L^{-1}\right) \tag{6}$$

and neglect upper order terms we get the approximate expression

$$p_{Lc,r(i)}^X \approx p_{\infty c,r(i)}^X + \chi_{Lc,r(i)}^X, \tag{7}$$

which are the regressions shown in Fig. 7 for cases I and III, where we have used the expected value 4/3 for the exponent ν. The linear regressions allow one to estimate the following values: $p_{\infty c,i}^I = 0.5553$, $p_{\infty c,r}^I = 0.5540$, $p_{\infty c,i}^{III} = 0.5534$, and $p_{\infty c,r}^{III} = 0.5521$. Similarly, we also obtained $p_{\infty c,i}^{II} = 0.5581$, $p_{\infty c,r}^{II} = 0.5583$, $p_{\infty c,i}^{IV} = 0.5513$, $p_{\infty c,r}^{IV} = 0.5583$, $p_{\infty c,i}^{V} = 0.5529$, and $p_{\infty c,r}^{V} = 0.5528$.

As it can be seen there are no great differences between results obtained by method A or method B. For the rest of the paper we will use just one percolation threshold for each size and deposition case corresponding to the mean value between the results given by these two methods: $p_{\infty c}^X$ (see second column of Table II).

Numerical. As already explained percolation is determined for 10^5 runs for each concentration p, on each lattice size L, for each deposition case ($X = I$–V), and for each percolation criterion ($Y = R, D, I, U, A$). Functions $R_{L,Y}^X(p)$ are reported

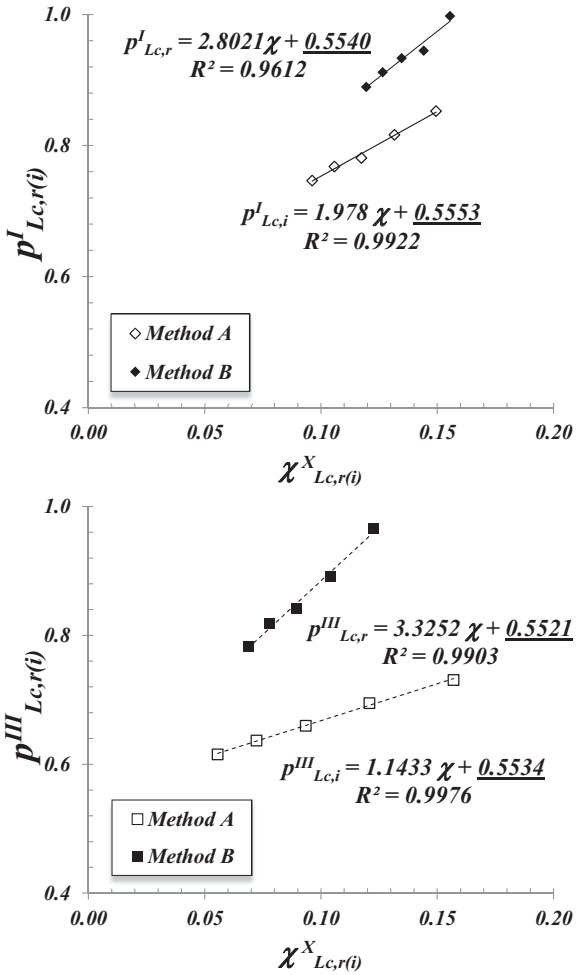

FIG. 7. Linear regressions to obtain percolation thresholds in the thermodynamic limit for case I at the top and for case III on the bottom. We have used the analytical value $\nu = 4/3$ to construct these plots.

in Fig. 8, for $X = I$ (empty symbols) and $X = III$ (solid symbols); percolation criteria are identified in the figure.

In order to express $R^X_{L,Y}(p)$ as a function of continuous values of p, it is convenient to fit $R^X_{L,Y}(p)$ with some approximating function through the least-squares method. The fitting curve is the *error function* because $dR^X_{L,Y}(p)/dp$ is

TABLE II. Analytical and numerical results of the parameters $p^X_{\infty c}$ and ν^X for site percolation corresponding to cases I, II, III, IV, and V.

	Analytical		Numerical	
Case	$p^X_{\infty c}$	ν	$p^X_{\infty c}$	ν
I	0.554	1.52	0.5279(1)	1.34(3)
II	0.558	1.53	0.5748(1)	1.34(1)
III	0.552	1.58	0.5708(1)	1.33(1)
IV	0.555	1.54	0.5527(1)	1.32(2)
V	0.553	1.41	0.5514(1)	1.34(1)

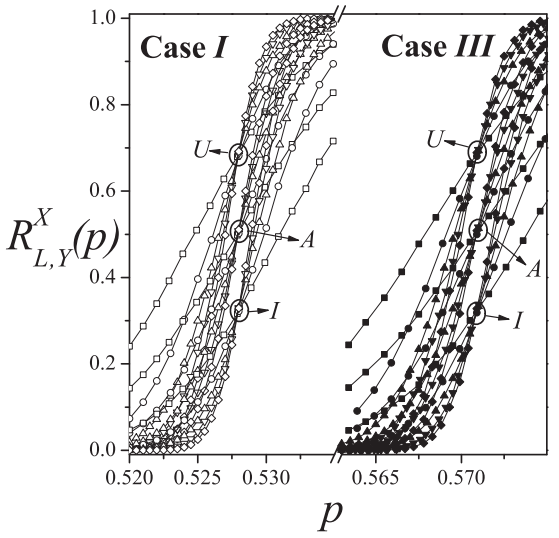

FIG. 8. Fraction of percolating lattices as functions of the concentration p for cases I (empty symbols) and III (solid symbols) and different values of L: 384, squares; 768, circles; 1152, up triangles; 1536, down triangles; 1920, diamonds. Criteria I, A, and U are indicated in the figure.

expected to behave like the Gaussian distribution [26]

$$\Lambda^X_{L,Y}(p) = \frac{dR^X_{L,Y}(p)}{dp} = \frac{1}{\sqrt{2\pi}\,\Delta^X_{L,Y}} \exp\left\{-\frac{1}{2}\left[\frac{p - p^X_{Lc,Y}}{\Delta^X_{L,Y}}\right]^2\right\}, \quad (8)$$

where $p^X_{Lc,Y}$ is the concentration at which the slope of $R^X_{L,Y}(p)$ is the largest and $\Delta^X_{L,Y}$ is the standard deviation from $p^X_{Lc,Y}$.

Table III collects the values of $p^X_{Lc,Y}$ obtained for criterion A and different lattice sizes L as indicated. Similar tables were obtained for the other percolation criteria; they are not included here for space reasons but the corresponding values will be used right below.

With previous results for $p^X_{Lc,Y}$, a scaling analysis can be done by the same approach used in the case of the analytical method, namely by means of Eqs. (6) and (5). However, since the lattices used in the numerical calculations are large enough we can avoid the small size corrections, keeping only coefficient a^X_Y as different from zero. This leads to the relationship [1]

$$p^X_{Lc,Y} = p^X_{\infty c,Y} + a^X_Y L^{-1/\nu}, \quad (9)$$

TABLE III. Values of $p^X_{Lc,Y}$ obtained for criterion A and different lattice sizes L as indicated in the text.

Case/L =	384	768	1152	1536	1920
I	0.52786	0.52798	0.52792	0.52793	0.52792
II	0.57499	0.57499	0.57500	0.57497	0.57498
III	0.57081	0.57089	0.57086	0.57085	0.57087
IV	0.55275	0.55273	0.55273	0.55272	0.55269
V	0.55135	0.55138	0.55142	0.55142	0.55140

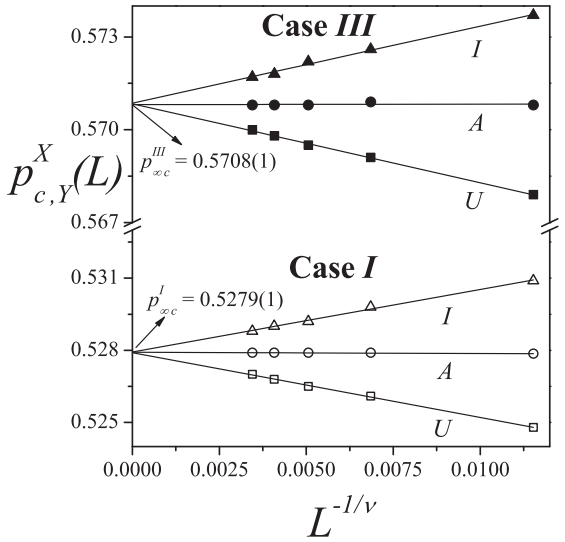

FIG. 9. Extrapolation of $p^X_{Lc,Y}$ towards the thermodynamic limit according to the analytical prediction given by Eq. (9) for the data in Fig. 8. Triangles, circles, and squares denote the values of $p^X_{Lc,Y}$ obtained by using the criteria I, A, and U, respectively.

where a^X_Y is a nonuniversal constant and ν is the critical exponent of the correlation length which will be taken as 4/3 for the present analysis, since, as it will be shown below, our model belongs to the same universality class as random percolation [1].

Figure 9 shows the plots towards the thermodynamic limit of $p^X_{Lc,Y}$ according to Eq. (9) for the data in Fig. 8. Cases I (empty symbols) and III (solid symbols) are presented, combined with criteria I (triangles), A (circles), and U (squares). From extrapolations it is possible to obtain $p^X_{\infty c,Y}$ for the criteria I, A, and U. Combining the three estimates for each case, the final values of $p^X_{\infty c}$ can be obtained. They are reported in the fourth column of Table II. Additionally, the maximum of the differences between $|p^X_{\infty c,U} - p^X_{\infty c,A}|$ and $|p^X_{\infty c,I} - p^X_{\infty c,A}|$ gives the error bar for each determination of $p^X_{\infty c}$. This error is given in parentheses in Table II.

The procedure of Fig. 9 was repeated for cases II, IV, and V. As it can be observed from the inspection of Table II, both analytical and numerical methods yield similar values for the percolation threshold, with differences under 5%. Small deviations can be attributed to the small size used in the analytical method and the possible error in the sample generation for the numerical studies.

B. Exponent ν

Analytical. Critical exponents are of importance because they describe the universality class of a system and allow for the understanding of the related phenomena. This is particularly true for exponent ν, which is where we focus our attention now. We can make use of the expression [21]

$$\ln L = \nu^X \ln \lambda^X_\infty, \tag{10}$$

where λ^X_∞ represents the maximum value of the first derivative of the percolation function at $p = p_c$ in the limit of a cell of infinite dimensions, for the different deposition cases.

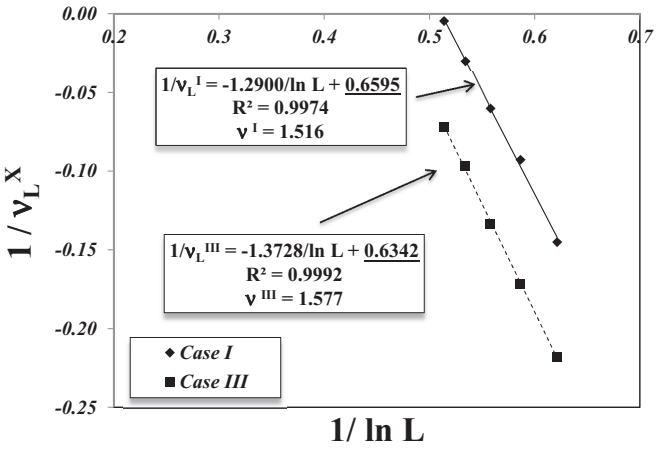

FIG. 10. Analytical results for exponent ν in cases I and III.

In the case of finite dimensions both ν and the maximum λ are size dependent, namely,

$$\ln L = \nu^X_L \ln \lambda^X_L\big(p^X_{c,i}\big). \tag{11}$$

We can follow the approach of Reynolds *et al.* [33] to write

$$\lambda^X_\infty = A^X_L \lambda^X_L\big(p^X_{c,i}\big), \tag{12}$$

where A^X_L is a parameter and $\lambda^X_L(p^X_{c,i})$ is the maximum value of the derivative at $p^X_{c,i}$ for lattices of size L and deposition case X, which we simply denote by $[\lambda^X_L]_{\max}$, dropping the index i since the inflection method is the only one used here:

$$\ln L = \nu\big(\ln A_L + \ln\big[\lambda^X_L\big]_{\max}\big), \tag{13}$$

which by means of Eq. (10) and reordering terms and factors leads to

$$\frac{1}{\nu^X_L} = -\frac{\ln A_L}{\ln L} + \frac{1}{\nu}. \tag{14}$$

This expression is a straight line when plotting $\frac{1}{\nu^X_L}$ vs $\frac{1}{\ln L}$, giving $\frac{1}{\nu}$ as the intercept on the ordinate axis in the thermodynamic limit. This is represented in Fig. 10 for the cases I and III, while all values of ν obtained in this way are given in the third column of Table II.

Numerical. The standard theory of finite-size scaling allows for various efficient routes to estimate ν from numerical data. One of these methods is from the maximum of the function in Eq. (8) [1],

$$\big[\Lambda^X_{L,Y}(p)\big]_{\max} \propto L^{1/\nu}. \tag{15}$$

In Fig. 11, $\ln\{[\Lambda^X_{L,A}(p)]_{\max}\}$ has been plotted as a function of $\ln\{L\}$ (note the log-log functional dependence) for cases I–V as indicated. According to Eq. (15) the slope of each line corresponds to $1/\nu$. As it can be observed, the slopes of the curves remain constant (and close to 3/4) for all studied cases.

An alternative way for evaluating ν is given through the divergence of the root-mean-square deviation of the threshold observed from their average values, $\Delta^X_{L,Y}$ in Eq. (8) [1],

$$\Delta^X_{L,Y} \propto L^{-1/\nu}. \tag{16}$$

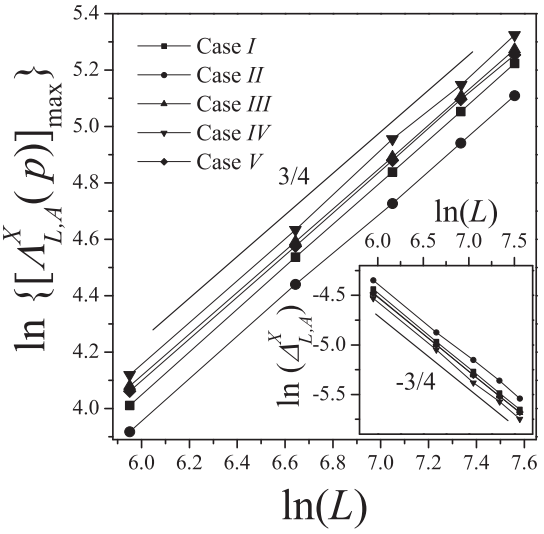

FIG. 11. $\ln\{[\Lambda^X_{L,A}(p)]_{\max}\}$ as a function of $\ln(L)$ for cases I–V as indicated. According to Eq. (15) the slope of each line corresponds to $1/\nu$. Inset: $\ln(\Delta^X_{L,A})$ as a function of $\ln(L)$ for cases I–V as indicated. According to Eq. (16), the slope of each curve corresponds to $-1/\nu$.

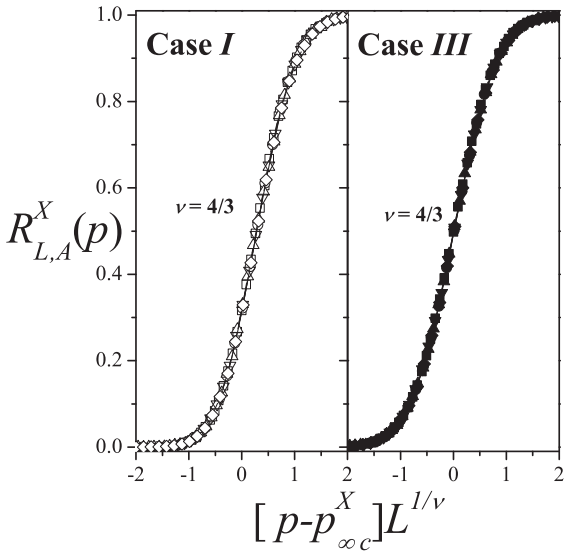

FIG. 12. Data collapse of the fraction of percolation samples $R^X_{L,A}(p)$ as a function of the argument $[p - p^X_{\infty c}]L^{1/\nu}$. Curves on the left(right) correspond to case I (III). For each case, different lattice sizes have been considered: 384, squares; 768, circles; 1152, up triangles; 1536, down triangles; 1920, diamonds.

The inset in Fig. 11 shows $\ln\{\Delta^X_{L,A}\}$ as a function of $\ln\{L\}$ (note the log-log functional dependence) for cases I–V. According to Eq. (16), the slope of each line corresponds to $-1/\nu$. As in the main figure, the slopes of the curves remain constant (and close to $-3/4$) for all studied cases.

The procedure in Fig. 11 was repeated for I and U percolation criteria. Thus six values of ν were obtained for each case: for either Eq. (15) or Eq. (16) we can have at least three possible percolation ways: $Y = I, U, A$. Averaging these six estimates, the final values of ν were obtained and collected in the fifth column of Table II. The results for the five deposition cases coincide within numerical errors with the exact value of the critical exponent of the ordinary percolation, namely, $\nu = 4/3$. This finding clearly indicates that this problem belongs to the universality class of random percolation regardless of the trimer shape considered.

The scaling behavior can be further tested by plotting $R^X_{L,Y}(p)$ vs $[p - p^X_{\infty c}]L^{1/\nu}$ and looking for data collapse. Using the values of $p^X_{\infty c}$ previously calculated and the exact value $\nu = 4/3$, an excellent scaling collapse was obtained for all trimer shapes. Figure 12 shows the curves corresponding to criterion A for cases I and III. This leads to independent control and consistency check of the numerical value for the critical exponent ν found above.

IV. CONCLUSIONS

Percolation thresholds for site trimer depositions were calculated by both analytical and numerical techniques. Critical concentration for percolation is close to 0.55, which is lower than dimer site percolation (0.56 [20]) and even smaller that monomer site percolation (0.59 [20,34]), showing a tendency: the percolation threshold decreases with the size of the k-mer.

The case of trimers under study allows one to consider different shape depositions. Extensive numerical methods allow one to find slightly different percolation thresholds depending on the shape of the site trimer. The largest percolation threshold is for the nematic case (0.5748) and the lowest one is for the straight case (0.5297). The analytical methods render a much lower dispersion around 0.55 probably due to the smallness of the cell sizes. The tendency commented here had been anticipated for some numerical depositions of long k-mers [8,9]; here we have established it for all possible trimer deposition possibilities by both analytical and numerical methods

Previous results open new lines of research as follows. Do all k-mer shapes always tend to the same percolation parameters? What is the percolation threshold as k grows? The answers to previous questions are almost impossible when considering all the growing shapes as k increases. However, we are already beginning calculations of percolation thresholds for straight and nematic cases which are the most general of all, since these shapes are present for any length of the polymer. From numerical calculations [12] the initial tendency is a decrease in the percolation threshold with an interesting return to higher values for $k < 13$. These behaviors have not been explored theoretically yet.

Another aspect of this problem which should deserve joint numerical and theoretical studies is jamming: at a certain coverage the filling of the lattice saturates and this phenomenon should be shape and size dependent for the k-mer. We are in the middle of extensive calculations including dimers and trimers which already sustain previous hypothesis.

Critical exponent ν obtained by numerical methods is close to 4/3: 1.34, 1.34, 1.33, 1.32, and 1.34 for cases I through V, respectively. In the analytical treatment some deviations are found due to the small size of the cells. Thus for instance 1.52 is obtained for case I, 1.58 for case III, and 1.41 for case V.

Generally speaking exponent ν is always close to 4/3 independently of the deposition case as determined by numerical

calculations. This result shows that this problem belongs to the universality class of random percolation. The determination of the exponent ν by means of the analytical method gives consistently values a bit larger than $4/3$, but this was already the situation when this same method was used for monomers (1.41) [20] and for dimers (1.49) [20]. This is apparently a size effect since, as the k-mer gets larger for cells of similar L, the discrepancy with the expected value $4/3$ increases.

The analytical methods used below point to the understanding of the phenomenon. However, the percolation results thus obtained are very close to those obtained by means of the extensive numerical calculations presented here giving consistency to the approach.

Moreover, in the case of the analytical approach two methods were used to obtain the percolation threshold and the results obtained are very similar between themselves. The values for the percolation threshold obtained by the renormalization cell are all very similar among them and close to 0.55.

ACKNOWLEDGMENTS

This work was supported in part by the following institutions in Argentina: CONICET under Project No. PIP 112-201101-00615, Universidad Nacional de San Luis under Project No. 322000, and the National Agency of Scientific and Technological Promotion under Project No. PICT-2010-1466. The numerical work was done using the BACO parallel cluster (composed by 50 PCs each with an Intel i7-3370/2600 processor) located at Instituto de Física Aplicada, Universidad Nacional de San Luis–CONICET. Partial support of the following Chilean agencies is also acknowledged: Dirección de Investigación de la Universidad de La Frontera (DIUFRO) under Contract No. DI 15-0011, the supercomputing infrastructure of the NLHPC (ECM-02) at Centro de Modelación y Computación Científica of Universidad de La Frontera, Fondecyt under Contract No. 1150019, and Financiamiento Basal para Centros Científicos y Tecnológicos de Excelencia (Chile) through the Center for Development of Nanoscience and Nanotechnology (CEDENNA) under Contract No. FB0807.

[1] D. Stauffer and A. Aharony, *Introduction to Percolation Theory* (Taylor & Francis, London, 1994).
[2] M. Sahimi, *Applications of Percolation Theory* (Taylor & Francis, London, 1994).
[3] J. Shao, S. Havlin, and H. E. Stanley, Phys. Rev. Lett. **103**, 018701 (2009).
[4] J. Goldenberg, B. Libai, S. Solomon, N. Jan, and D. Stauffer, Physica A **284**, 335 (2000).
[5] M. Girardi and W. Figueiredo, J. Chem. Phys. **120**, 5285 (2004).
[6] M. Cieśla and J. Barbasz, J. Mol. Model. **19**, 5423 (2013).
[7] P. N. Suding and R. M. Ziff, Phys. Rev. E **60**, 275 (1999).
[8] V. Cornette, A. J. Ramirez-Pastor, and F. Nieto, Physica A **327**, 71 (2003).
[9] V. Cornette, A. J. Ramirez-Pastor, and F. Nieto, Eur. Phys. J. B **36**, 391 (2003).
[10] G. D. Garcia, F. O. Sanchez-Varretti, P. M. Centres, and A. J. Ramirez-Pastor, Eur. J. Phys. B **86**, 403 (2013).
[11] Y. Leroyer and E. Pommiers, Phys. Rev. B **50**, 2795 (1994).
[12] Y. Y. Tarasevich, N. I. Lebovka, and V. V. Laptev, Phys. Rev. E **86**, 061116 (2012).
[13] V. A. Cherkasova, Y. Y. Tarasevich, N. I. Lebovka, and N. V. Vygornitskii, Eur. Phys. J. B **74**, 205 (2010).
[14] P. Longone, P. M. Centres, and A. J. Ramirez-Pastor, Phys. Rev. E **85**, 011108 (2012).
[15] D. A. Matoz-Fernandez, D. H. Linares, and A. J. Ramirez-Pastor, Eur. J. Phys. B **85**, 296 (2012).
[16] C. Brosseau, A. Beroual, and A. Boudida, J. Appl. Phys. **88**, 7278 (2000).
[17] F. Du, J. E. Fischer, and K. I. Winey, J. Polym. Sci. B **41**, 3333 (2003).
[18] T. Natsuki, M. Endo, and T. Takahashi, Physica A **352**, 498 (2005).
[19] J. L. Mietta, R. M. Negri, and P. I. Tamborenea, J. Phys. Chem. C **118**, 20594 (2014), and references therein.
[20] W. Lebrecht, J. F. Valdés, E. E. Vogel, F. Nieto, and A. J. Ramirez-Pastor, Physica A **392**, 149 (2013).
[21] W. Lebrecht, J. F. Valdés, E. E. Vogel, F. Nieto, and A. J. Ramirez-Pastor, Physica A **398**, 234 (2014).
[22] J. Carrasco, A. Hodgson, and A. Michaelides, Nat. Mater. **11**, 667 (2012).
[23] Ö. Can and N. B. Holland, Biochemistry **52**, 8745 (2013).
[24] C. W. Liu, G. L. Hou, W. J. Zheng, and Y. Q. Gao, Theor. Chem. Acc. **133**, 1550 (2014).
[25] J. Hoshen and R. Kopelman, Phys. Rev. B **14**, 3438 (1976).
[26] F. Yonezawa, S. Sakamoto, and M. Hori, Phys. Rev. B **40**, 636 (1989).
[27] K. Binder, Rep. Prog. Phys. **60**, 487 (1997).
[28] M. Z. Bazant, Physica A **316**, 29 (2002).
[29] E. E. Vogel, W. Lebrecht, and J. F. Valdes, Physica A **389**, 1512 (2010).
[30] D. Staufer, *Introduction to Percolation Theory* (Taylor & Francis, London, 1985).
[31] D. ben-Avraham and S. Havlin, *Diffusion and Reactions in Fractals and Disordered System* (Cambridge University Press, Cambridge, UK, 2000).
[32] P. M. C. de Oliveira, R. A. Nóbrega, and D. Stauffer, Braz. J. Phys. **33**, 616 (2003).
[33] P. J. Reynolds, H. E. Stanley, and W. Klein, Phys. Rev. B **21**, 1223 (1980).
[34] M. J. Lee, Phys. Rev. E **78**, 031131 (2008).